2nd International Symposium on Seawater Drag Reduction
Busan, Korea, 23–26 MAY 2005

Experimental Results on the Effect of Wall–Parallel Lorentz Forces on Lift and Drag of Hydrofoils

T. Weier, G. Gerbeth (Forschungszentrum Rossendorf, Germany)

ABSTRACT

The influence of wall–parallel Lorentz forces on the suction side flow of NACA 0015 and PTL IV hydrofoils is investigated experimentally. Emphasis is placed on separation control. Steady as well as time periodic Lorentz forces will be discussed. Their effect is compared mainly in respect of the attainable increase of the maximum lift and in terms of power consumption.

INTRODUCTION

Flow separation may cause an increase in form drag as well as considerable diminished lift on hydrofoils. Therefore it is usually an unwanted flow feature. Since separation is not unique to hydrofoils, but a rather common problem, a large variety of separation control methods have been developed. Among the more common ones are, e.g., jet blowing, suction, vortex–generators and wall-motion. For an overview see Gad–el–Hak and Bushnell (1991). Recent results with a focus on the use of periodic addition of momentum are reviewed by Greenblatt and Wygnanski (2000).

An electrically conducting fluid like seawater opens the additional possibility to use an electromagnetic, i.e. Lorentz force, to influence the flow. The Lorentz force density $\mathbf{F}$ appears as a body force term on the right hand side of the Navier–Stokes–Equation for incompressible flow

$$\frac{\partial \mathbf{u}}{\partial t} + (\mathbf{u}\cdot\nabla)\mathbf{u} = -\frac{p}{\rho} + \nu\nabla^2\mathbf{u} + \frac{\mathbf{F}}{\rho}, \tag{1}$$

where $\mathbf{u}$ denotes the velocity, p the pressure, and t the time, respectively. ρ is the density and ν the kinematic viscosity of the fluid. As can be seen from (1), the electromagnetic force density acts as a momentum source for the flow. The Lorentz force density itself is the vector product of a current density $\mathbf{j}$ and a magnetic induction $\mathbf{B}$

$$\mathbf{F} = \mathbf{j}\times\mathbf{B}. \tag{2}$$

Ohm's law

$$\mathbf{j} = \sigma(\mathbf{E} + \mathbf{u}\times\mathbf{B}) \tag{3}$$

for moving conductors describes the current density. $\mathbf{E}$ denotes an electric field, and σ the electrical conductivity of the fluid.

In liquid metal Magnetohydrodynamics (MHD), the Lorentz force density and the flow are usually strongly coupled, since the flow induces currents via the $\mathbf{u}\times\mathbf{B}$ term in (3), these currents generate Lorentz forces (2), and the Lorentz forces change the flow (1). The reason for this strong coupling is the very high electrical conductivity of liquid metals, typically $\sigma = O(10^6)$ S/m.

In the case of seawater and other electrolytes, σ is small (~ 10 S/m). Therefore, the induced currents are very low for moderate applied magnetic fields ($B_0 \sim 1$ T). Accordingly, the Lorentz forces due to these currents are negligible and too weak to act on the flow. In order to generate forces large enough to influence the flow, an additional electric field has to be applied. The ratio of the applied E_0 to the electric field induced by the free stream velocity U_∞ in the presence of the applied magnetic field B_0 is commonly termed load factor (Sutton and Sherman, 1965)

$$\phi = \frac{E_0}{U_\infty B_0}. \tag{4}$$

For seawater flow control with moderate magnetic fields, it follows from the above

$$\phi \gg 1. \tag{5}$$

This implies on one hand that the force density distribution can be calculated independently of the flow field. On the other hand, a large load factor means a small efficiency of momentum generation as will be discussed in more detail later.

Strictly speaking, the flow acts not only on the electric field distribution, but deforms the magnetic field as well. However, even in the case of most liquid metal MHD problems – apart from dynamo experiments – it is well justified to ignore the induced magnetic fields when determining the generated Lorentz force.

The Lorentz force as a type of actuator has several appealing features: momentum is directly generated in the fluid without associated mass flux, the frequency response

of the actuation is practically unlimited, no moving parts are involved. To quote Shercliff (1965): "MHD has a peculiar attraction for aerodynamicists and mechanical engineers; instead of being confined to pushing at the edges of fluid streams, they are enabled by MHD to grab the fluid in midstream!". Notwithstanding these advantages, experimental results on the use of Lorentz forces in fluids of low conductivity are somewhat scarce and practical applications – to the knowledge of the authors – limited to YAMATO–1, a surface ship equipped with two MHD thrusters (Motora and Takezawa, 1994). Without further references to MHD propulsion, which is a subject in its own right, first investigations of the electromagnetic control of electrolyte flows date back to the 1950's. Already in 1954, Crausse and Cachon gave experimental evidence of successful separation postponement as well as separation provocation on a half cylinder. Similar experiments were performed by Lielausis (1961). Rossow (1957) and Resler and Sears (1958) discussed aerospace applications of Lorentz forces in ionized air, among other things, to control heat transfer to reentry vehicles. A few investigations on laminar flow control (Gailitis and Lielausis, 1961; Tsinober and Shtern, 1967) and related topics (Meyer, 1967; Shtern, 1970) have been published later on, but the activities declined with the beginning 1970's. A renewed interest in electromagnetic flow control for low conducting fluids arose in the 1990's. The majority of papers dealt with skin friction reduction of turbulent boundary layers. For this purpose, different force configurations have been investigated. Nosenchuck and Brown (1993), O'Sullivan and Biringen (1998), Thibault and Rossi (2003), and others used nominally wall normal, time dependend forces. While a turbulent skin friction reduction of 55% was found for that case by Nosenchuck et al. (1995), other groups were unable to reproduce these results (Du et al., 2002). However, the real force distribution produced by the electromagnetic tiles is quite complex and may play a crucial role (Rossi and Thibault, 2002). Wall parallel forces in streamwise direction have been applied, e.g., in the experiments of Henoch and Stace (1995) and Weier et al. (2001) as well as in the numerical analysis of Crawford and Karniadakis (1997). This force configuration increases wall shear stress, because the acceleration of the near wall fluid leads to a higher slope of the mean velocity profile in streamwise direction. However, the momentum gain due to the Lorentz force surpasses the friction drag rise. Time dependent wall parallel forces in spanwise direction have been investigated numerically by, among others, Berger et al. (2000), and Du et al. (2002) and experimentally by Pang and Choi (2004), and Breuer et al. (2004). Drag reductions ranging from 10% for the directly measured mean drag coefficient (Breuer et al., 2004) to 40% for the local skin friction (Pang and Choi, 2004) have been found, indicating that this type of forcing is indeed

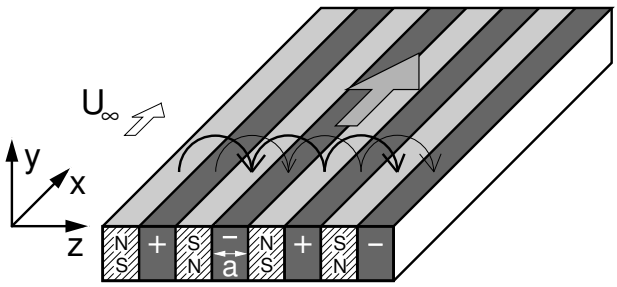

Figure 1: Electrode/magnet–array to generate a wall–parallel Lorentz force in streamwise direction.

able to reduce skin friction drag of turbulent flows. Nevertheless, the energy balance of the approach is not favorable.

Compared to skin friction reduction, the use of Lorentz forces to control flow separation received much less attention. Successful electromagnetic control of the flow around a circular cylinder has been reported by Petit (1983) for electrodes embedded in the cylinder and an externally applied magnetic field. A circular cylinder equipped with electrodes as well as permanent magnets generating a wall parallel force in streamwise direction was used in the experiments and numerical calculations of Weier et al. (1998). Similar configurations have later been investigated by Kim and Lee (2000), Posdziech and Grundmann (2001), and Chen and Aubry (2005). While skin friction drag is increased by this force configuration, form drag is strongly reduced for an initially separated flow at Reynolds numbers $Re = O(100)$. For stronger forcing, the increase in skin friction drag dominates the form drag decrease. The total drag on the cylinder under these conditions is, however, negative due to the electromagnetically generated thrust. Very recently, Shatrov and Gerbeth (2005) have shown that it is possible to reduce the drag of a sphere by three orders of magnitude using an optimized field distribution.

The paper at hand presents experimental results on separation control at hydrofoils with steady as well as time periodic wall parallel Lorentz forces. Additional information on details of the experimental setup can be found in Weier et al. (2003) for the steady and in Weier and Gerbeth (2004) for the time periodic case.

FORCE CONFIGURATIONS

Gailitis and Lielausis (1961) and Rice (1961) proposed the arrangement of flush mounted electrodes and permanent magnets shown in Fig. 1 to generate a wall parallel Lorentz force in the fluid above the plate. Magnets and electrodes are of the same width a, a condition maximizing the attainable integral force density (Grienberg, 1961). Apart from end effects, both electric as well as

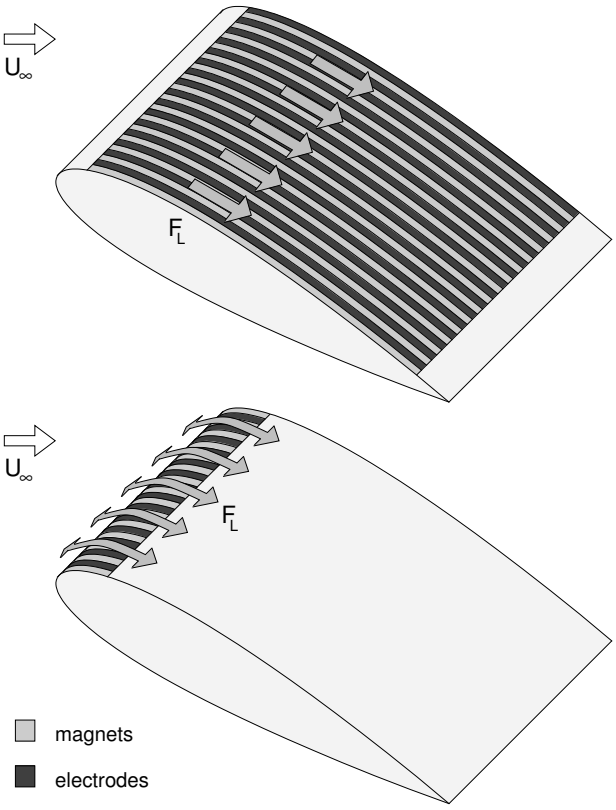

Figure 2: Electrode/magnet–array for stationary momentum input extending almost over the full suction side (top) and short electrode/magnet–array at the leading edge for time periodic forcing (bottom).

magnetic fields have only components in wall normal (y) and spanwise (z) direction. From the vector product (2) follows that the Lorentz force possesses a streamwise (x) component F_x only. The force density distribution shows non–uniformities in z–direction in the range of $0 \leq y \lesssim a$ (Weier et al., 2001). Averaged over z, the mean force density decreases exponentially with increasing wall distance

$$F_x = \frac{\pi}{8} j_0 M_0 e^{-\frac{\pi}{a}y}. \tag{6}$$

M_0 denotes the magnetization of the permanent magnets and j_0 the applied current density, respectively. The magnetic induction B_0 at the surface of the magnetic poles can be calculated from the geometry of the magnets and their magnetization M_0. For magnets infinitely extended in $(-y)$–direction, $B_0 = M_0/2$ holds (Avilov, 1998).

The electrode/magnet array sketched in Fig. 1 can be applied to the suction side of hydrofoils as shown in Fig. 2. Two different configurations have been used for stationary and time periodic forcing of the suction side flow. The main parameters of the hydrofoils are summarized in table 1. Stationary forcing directly balances the momentum deficit of the suction side flow, while time periodic forcing aims to enhance momentum transport between the free stream flow and the wall near region. Since the purpose of actuation is different in both cases, the actuators, i.e. the electrode/magnet–arrays, differ from each other. For steady momentum input, the actuator extends over almost the whole suction side as shown in the top part of Fig. 2. This results in the lowest ohmic resistance of the arrangement for a fixed total momentum input. According to Avilov (1998), the ohmic resistant R of the fluid above the electrodes can be written as

$$R = \frac{4a}{s(x_e - x_s)\sigma}. \tag{7}$$

Here, s denotes the span of the hydrofoil and x_s and x_e beginning and end of the electrode/magnet–array along the chord line, respectively. It is always assumed that the actuator extends over the whole span. Oscillatory forces, which can be seen as analogous to periodic tangential blowing and suction, are effective only when applied near the separation point, as has been shown for acoustic excitation by Hsiao et al. (1990). Consequently, the actuator extends only over a short region near the leading edge of the hydrofoil as shown in the bottom part of Fig. 2.

A momentum coefficient defined in analogy to that used in separation control by blowing (Poisson-Quinton, 1956) is a suitable parameter to characterize the effect of electromagnetic forces (Weier et al., 2003) on the flow. The momentum coefficient for stationary forces

$$c_\mu = \frac{1}{2} \cdot \frac{a j_0 B_0}{\rho U_\infty^2} \cdot \frac{x_e - x_s}{c} \tag{8}$$

relates the total moment input by the Lorentz force to the product of dynamic pressure and foil surface.

	PTL IV		NACA 0015	
	S	L	S	L
c/mm	158	158	160	667
s/mm	345	360	240	1088
s/c	2.18	2.28	1.5	1.63
a/mm	5	10	5	10
a/c	0.03	0.06	0.03	0.015
x_s/mm	6	12	0	25
x_e/mm	134	131	15	563
B_0/T	0.2	0.4	0.33	0.58
forces	stat./peri.	stat.	peri.	stat.

Table 1: Parameters of the hydrofoils used in the experiments. c... chord length; s... span; a... electrode width; x_s, x_e ... beginning and end of electrode/magnet–array; B_0... magnetic induction at the magnets surface; stat.... stationary; peri.... periodic.; S, L... index for small and large versions.

In the case of oscillatory forces, which are readily generated by feeding the electrodes with alternating current, the effective momentum coefficient

$$c'_\mu = \frac{1}{2} \cdot \frac{a j'_0 B_0}{\rho U_\infty^2} \cdot \frac{x_e - x_s}{c} \tag{9}$$

expressed with the effective current density

$$j'_0 = \sqrt{\frac{1}{T} \int_0^T j_0(t)^2 \, \mathrm{d}t} \tag{10}$$

is used to characterize the Lorentz force influence. $j_0(t)$ denotes the time–dependent applied current density and T is the period of oscillation. With the excitation frequency $f_e = 1/T$ a forcing Strouhal number as a second parameter for the time dependent forcing can be defined as follows

$$St_e = \frac{f_e c}{U_\infty}. \tag{11}$$

STEADY LORENTZ FORCES

In the following, the usual definitions of lift C_L and drag C_D coefficient,

$$C_L = \frac{F_L}{\frac{\rho}{2} U_\infty^2 cs} \quad \text{and} \quad C_D = \frac{F_D}{\frac{\rho}{2} U_\infty^2 cs} \tag{12}$$

will be used. Here F_L denotes the lift and F_D the drag force, respectively. At zero angle of attack α, no lift force acts on a symmetric airfoil like the PTL IV and NACA 0015 used here. On a sufficiently slender foil, no separation would be expected. Fig. 3 shows the effect of a single–side Lorentz force on lift and drag of the NACA 0015_L at different chord length Reynold numbers. A straight line of

$$C_D = 0.0239 - 1.01 \cdot c_\mu \tag{13}$$

can be fitted to the measured values of the drag coefficient. The slope of the linear relation equals almost exactly to minus one. That is, the thrust generated by the Lorentz force drives the hydrofoil very efficiently. In fact, the reduction of the measured drag is even a little larger than the Lorentz force generated thrust, which should be attributed to an underestimation of the Lorentz force actually applied. Since the initial drag of the foil is low, the total drag of the hydrofoil is negative for most c_μ values.

Due to the asymmetric acceleration of the flow, circulation is generated. This leads to a lift force increasing with the momentum coefficient. The measured lift coefficients can be described by the following fit

$$C_L = 0.843 \cdot c_\mu^{0.521}. \tag{14}$$

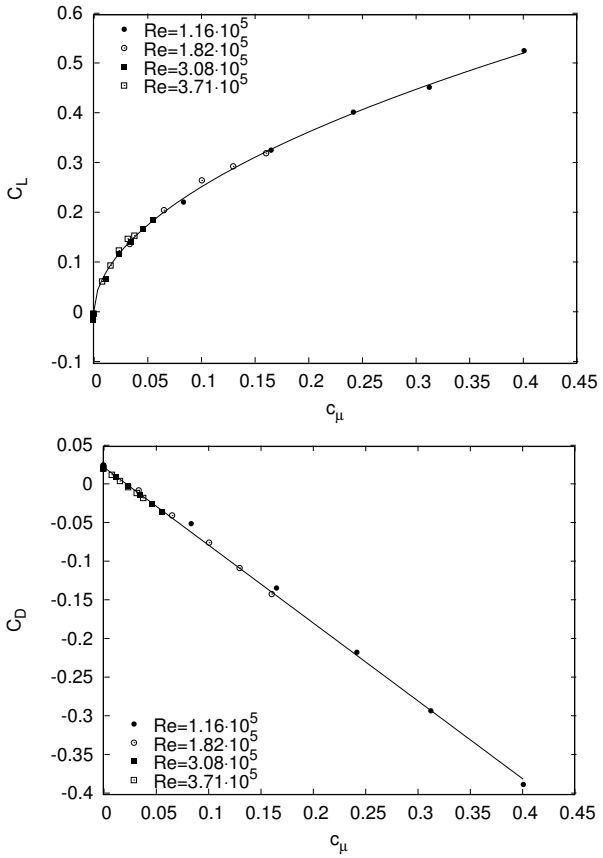

Figure 3: Lift- (top) and drag coefficient (bottom) *versus* c_μ for a NACA 0015 at $\alpha = 0°$ and different Reynolds numbers with fits (13) and (14).

Hence, as shown in the top part of Fig. 3, a scaling as approximately $C_L \sim \sqrt{c_\mu}$ has been found. This indicates a similar behaviour as found in the case of circulation control by blowing (Siestrunck, 1961).

Fig. 4 gives drag and lift values for a NACA 0015 at 18° of attack. The flow is attached except for $c_\mu = 0$ and the two lower Reynolds numbers of $Re = 1.15 \cdot 10^5$ and $Re = 1.82 \cdot 10^5$. As in the case of the hydrofoil in parallel flow, the drag coefficient depends linearly on the momentum coefficient with the exceptions mentioned before. Disregarding these values, a straight line fit results in

$$C_D = 0.229 - 1.07 \cdot c_\mu. \tag{15}$$

Again, the slope of this line equals to one in good approximation. The proportionality of the lift coefficient and the square root of the momentum coefficient can be detected likewise:

$$C_L = 1.02 + 2.26 \cdot c_\mu^{0.478}. \tag{16}$$

Since the inclination angle is relatively high, both the initial lift coefficient and the multiplier are larger than those

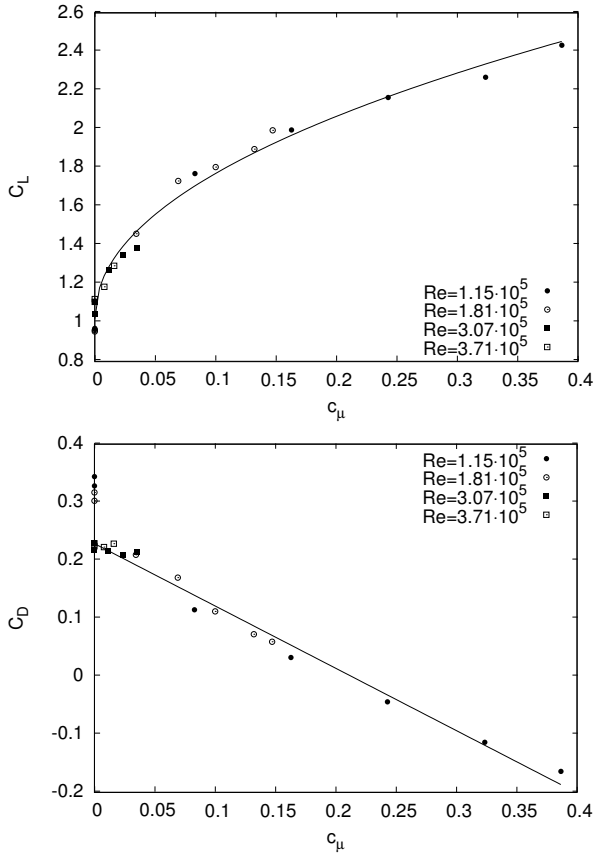

Figure 4: Lift- (top) and drag coefficient (bottom) *versus* c_μ for a NACA 0015 at $\alpha = 18°$ and different Reynolds numbers with fits (15) and (16).

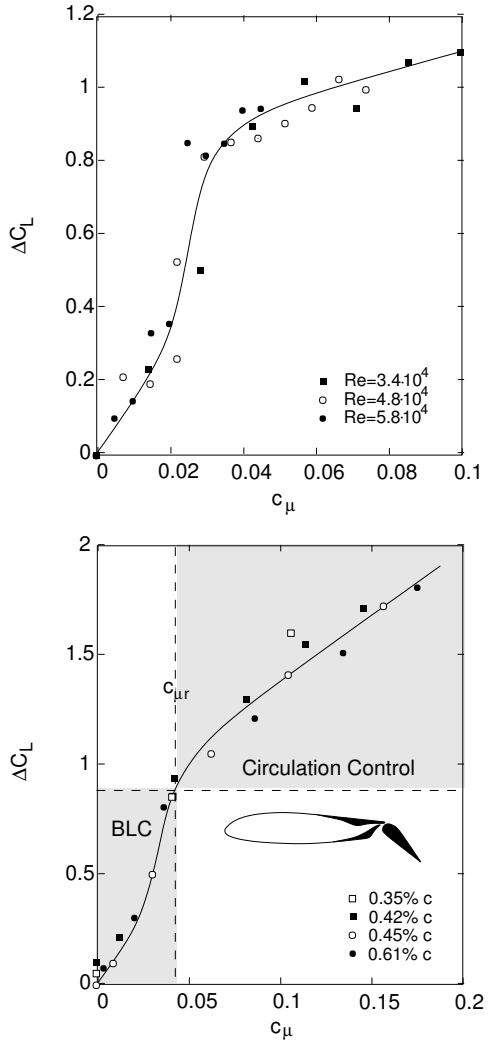

Figure 5: Lift increase versus momentum coefficient for an electromagnetically controlled hydrofoil at 17 ° (top) and for steady blowing over a 45° inclined flap on a NACA 23015 according to Schwier (1943) and Poisson-Quinton (1956) (bottom).

for $\alpha = 0°$. While the first is evident, the latter is similar to the findings in circulation control by blowing. At lower Reynolds numbers, a 17° inclined PTL IV_L is already stalled. The top part of Fig. 5 shows the lift increment with increasing momentum coefficient. In comparison to the graphs in Figs. 3 and 4 the dependency is more complex. At small momentum coefficients, the lift increase is steep, while it flattens for higher c_μ. It may be helpful to compare the findings again with results from separation control by blowing. On the right hand side of Fig. 5, ΔC_L versus c_μ values for blowing over a flap are given according to Schwier (1943) and Poisson-Quinton (1956). Schwier (1943) used a NACA 23015 in parallel flow with a 45° deflected flap. A jet was blown from a slit over the flap shoulder. Poisson-Quinton (1956) rearranged Schwiers measurements using the momentum coefficient as a parameter for the blowing intensity. This collapsed Schwiers values fairly well. Two different regimes can be identified, boundary layer control (BLC) for small values of the momentum coefficient and circulation control for large c_μ. The corresponding parts of the figure are shaded gray. In the boundary layer control regime, a gradual reattachement of the separated flow over the flap takes place. This leads to a comparatively large increase of the lift coefficient. The momentum coefficient corresponding to complete reattachement $c_{\mu r}$ marks the upper end of the boundary layer control regime. At $c_\mu > c_{\mu r}$ the lift gain is smaller and proportional to $\sqrt{c_\mu}$, circulation control dominates the flow.

It would appear that the same classification may be applied to the upper part of Fig. 5 showing electromagnetic separation control. Even the numerical values of ΔC_L and $c_{\mu r}$ match surprisingly well, though this should be attributed to pure chance, since the flow conditions are quite

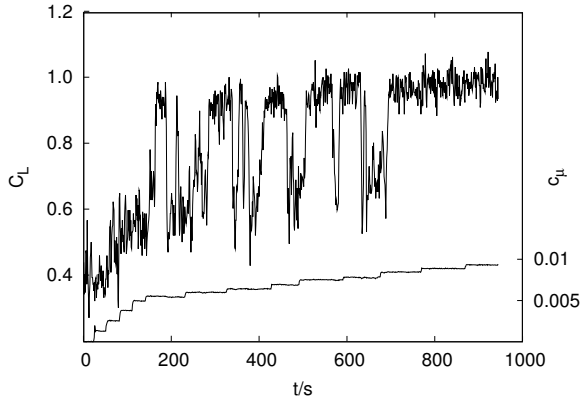

Figure 6: C_L and c_μ for the PTL IV$_S$ at $\alpha = 16°$ and $Re = 5.7 \cdot 10^4$ *versus* time.

different in both cases. However, the general trends are obviously the same.

While mean values of the lift coefficient are given in Fig. 5, Fig. 6 reveals the instationary nature of the reattachement process showing the 10 Hz sampled time signal of lift and momentum coefficient for the 16° inclined PTL IV$_S$ at a Reynolds number of $Re = 5.7 \cdot 10^4$. At small values of the momentum coefficient, the lift increases steadily. From $c_\mu \approx 0.0056$ onwards, the lift coefficient oscillates between two values, which might be assigned on the one hand to a separated and on the other hand to a reattached flow. The erratic lift increment is about twice as large as the former increase due to $c_\mu \approx 0.0056$. This regime of large amplitude oscillations merges into a stable state for $c_\mu \gtrapprox 0.0084$. A further increase of the injected momentum results only in weak lift increases, the circulation control regime is reached. $c_{\mu r}$ is noticeable smaller than for the PTL IV$_L$, although the angles of attack corresponding to Figs. 5 and 6 differ only slightly. This is most likely due to the different electrode materials used. While the PTL IV$_S$ is equipped with corrosion resistant RuO_2/IrO_2 covered titanium electrodes, the PTL IV$_L$ features relatively rapidly corroding stainless steel electrodes. Since the electrodes partly form the foils surface, corrosion there leads to surface deformations. Caused by these deformations, present only on the PTL IV$_L$, both hydrofoils may be much less similar than expected.

Both effects, separation and circulation control, are evident also in the C_L versus α and C_D–α curves shown in Fig. 7. Only points at $\alpha = 1°$ and around the stalling angle have been measured for the NACA 0015. As already shown, at small angles of attack, the suction side Lorentz force increases lift and decreases drag, the corresponding measurement points are shifted accordingly. At higher angles of attack, separation prevention gains importance. Due to the Lorentz force acting as a source of momentum

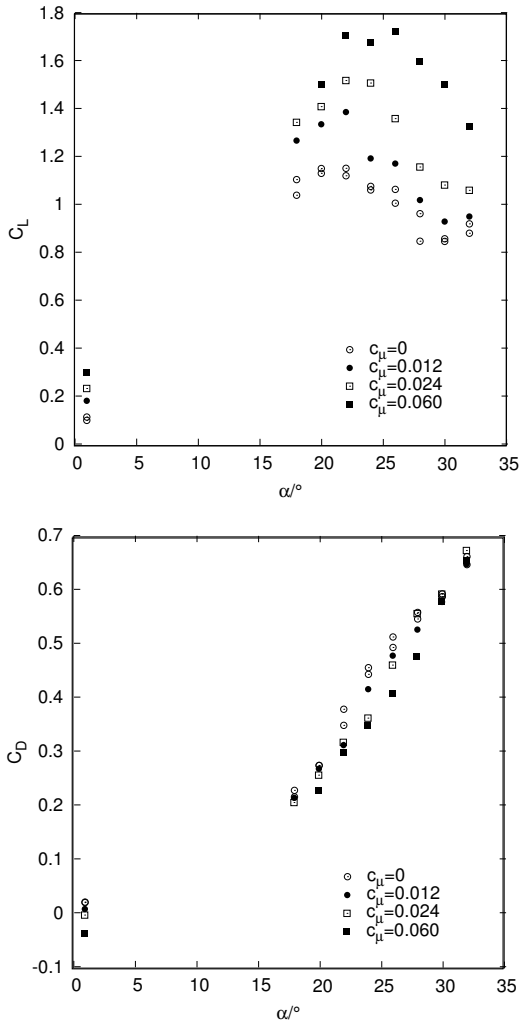

Figure 7: Lift and drag coefficient for the NACA 0015 *versus* angle of attack at $Re = 3.0 \cdot 10^5$.

for the near wall flow, stalling takes place at higher angles of attack then in the unforced case. Therefore, a higher maximum lift corresponding to the higher maximum angle of attack can be established. Obviously, also the type of stall is influenced by the suction side Lorentz force. While the loss of lift is relatively moderate for the unforced NACA 0015$_L$, it is larger and abrupt for the forced hydrofoil. The drag of the forced foil is always smaller than that of the unforced, most pronounced when the unforced flow is separated while the forced flow remains attached.

Scaling relations for the maximum attainable lift gain

$$\Delta C_{L\max} = C_{L\max}(c_\mu) - C_{L\max}(c_\mu = 0) \qquad (17)$$

as a function of the momentum coefficient have been obtained in Weier et al. (2003). For the meaning of this quantity see also the sketch in Fig. 15. A simple power law fit

of the available measurements results in

$$\Delta C_{L\max} = 2.91 \cdot c_\mu^{0.544}. \quad (18)$$

The exponent of c_μ is very near to 0.5, suggesting that circulation control plays an important role in the parameter range investigated.

At $Re \sim 10^5$ lift increments of $\Delta C_{L\max} \sim 1$ have been reached on the various hydrofoils. Such a lift increase is of definite interest for ship components. However, extrapolating the measured data to velocities of typical naval applications reveals that power demand may become a critical issue.

TIME PERIODIC LORENTZ FORCES

Separation control through periodic addition of momentum offers a reduction of the cost, in terms of momentum input, by up to 2 orders of magnitude for the same control effect compared to stationary action (see e.g. Greenblatt and Wygnanski, 2000). It seems an obvious consequence to apply time periodic Lorentz forces with the expectation of a similar gain in efficiency. Since the mechanism of periodic forcing is supposed to be connected to shear layer excitation, the actuator should be placed near the separation line as shown in the bottom part of Fig. 2. Flow visualizations given in Weier and Gerbeth (2004) show that the otherwise fully separated suction side flow can be reattached in an averaged sense by a time periodic Lorentz force acting near the leading edge.

Fig. 8 gives an overview of the forcing effect at various frequencies, momentum coefficients and different angles of attack. At the low Reynolds number of $Re = 5.2 \cdot 10^4$, the hydrofoil stalls already at the low angle of attack $\alpha = 13°$. At $\alpha = 14°$ the lift coefficient has only half the value of the attached case, indicating abrupt leading edge stall typical for this low Reynolds number range. Baseline values of C_L and C_D are plotted at $St_e = 0$. Excitation with a relatively small amplitude of $c'_\mu = 0.14\%$ is able to restore the lift of the attached flow. It seems as an obvious assumption to interpret this effect as the result of a boundary layer transition triggered by the forcing. This belief is corroborated by the fact that the effect is nearly independent of the excitation frequency. Under excitation, lift and drag coefficient are nearly constant up to $St_e = 50$ (not shown), i.e. in the full range of frequencies investigated. An increase of the momentum coefficient raises the lift coefficient only slightly, but the drag more pronounced. The latter might be caused by an intensified momentum transfer in the boundary layer due to the excitation. If the flow was already attached to the major part of the hydrofoil, the further increase of excitation amplitude would not cause a distinct change in the lift.

At an inclination angle of $\alpha = 17°$ and $Re = 8.0 \cdot 10^4$, the flow behaviour changes. For momentum coefficients $c'_\mu \leq 0.23\%$, a strong influence of the excitation frequency on lift as well as on drag is detectable. Both reach maximum values at $St_e = 0.75$. The forcing effect decreases relatively rapidly towards higher as well as lower frequencies. The shape of the C_L versus St_e curve is very similar to those observed for oscillatory leading edge blowing on a NACA 63_3–018 by Hsiao et al. (1990) and a NACA 0015 by Wygnanski and Seifert (1994). It is a generally accepted conception that this frequency dependency can be explained by the behaviour of the excited shear layer between the freestream and the separated flow, see Greenblatt and Wygnanski (2000); Hsiao et al. (1990). The shear layer will amplify the imposed disturbances in such a way that mixing and momentum transport between mean flow and separated region are enhanced. If the entrainment caused by this process is large enough, the shear layer will reattach to the boundary in a manner similar to the Coanda effect. According to this theory, the most effective forcing occurs at an St_e in the order of 1. For momentum coefficients $c'_\mu \geq 0.23\%$, the lift maximum at $St_e = 0.75$ is still present, but much less pronounced. Instead, forcing in the investigated frequency range of $0.25 \leq St_e \leq 50$ is nearly equally effective (frequencies $St_e > 8$ are not plotted). At $c'_\mu = 0.23\%$ itself, the flow regime seems very sensitive to initial conditions, different runs with this parameter exhibit either a strong or a weak dependence of the force coefficients on the excitation frequency. The maximum lift coefficient in the case of a weak frequency influence is larger ($C_L = 1.04$) than in the case where the flow shows a strong dependence on the excitation frequency ($C_L = 0.93$). It may be an admissible hypothesis to attribute the change in the C_L versus St_e curve to a transition between two different flow regimes. At small momentum coefficients, the excitation of the mixing layer seems to dominate the flow, while a stronger forcing seems to be able to completely reattach the boundary layer. In the time resolved force measurements, the forcing frequency is very dominant for $St_e \leq 0.75$ and $c'_\mu \leq 0.23\%$. Though it is still discernible for $c'_\mu \geq 0.23\%$, the rms value relative to the mean lift is about four times smaller than at lower momentum coefficients. While the mean drag is slightly increased for low St_e and low c'_μ compared to the unforced case, it drops by about 30% for $c'_\mu \geq 0.23\%$. The assumption of two different flow regimes is supported by flow visualizations on a Sikorsky SSC–A09 airfoil section at $Re = 2.5 \cdot 10^5$ reported by McCormick (2000). That author found at post–stall angles of attack for $c'_\mu = 0.5\%$ a flow dominated by large coherent structures, but reattached in an averaged sense. The situation changes for $c'_\mu = 1.5\%$. At that momentum coefficient the smoke visualization shows a fully attached flow without visible coherent structures.

The bottom part of Fig. 8 gives lift and drag coefficients for $Re = 5.2 \cdot 10^4$ and $\alpha = 20°$. At these parameters the

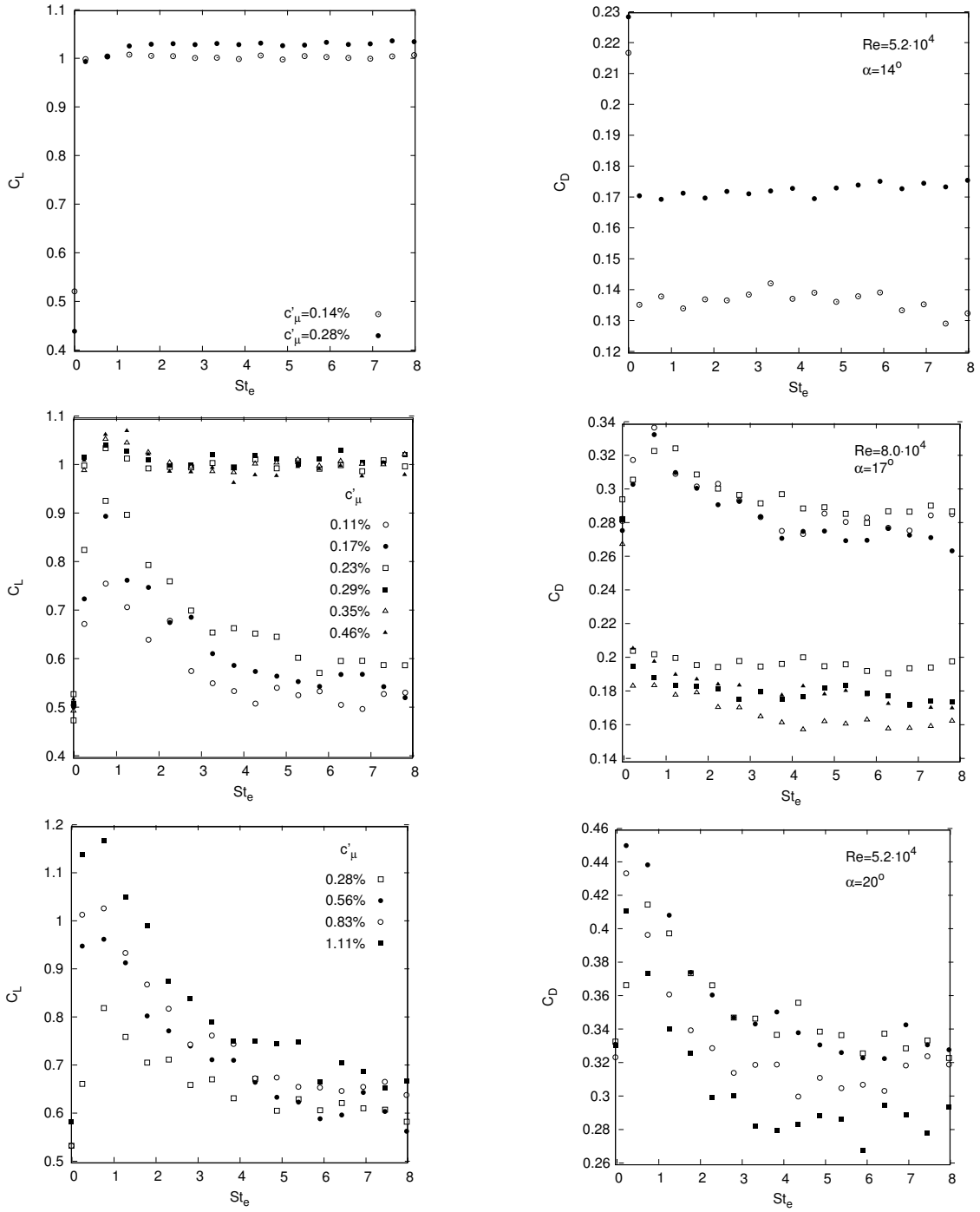

Figure 8: Influence of the excitation frequency on C_L and C_D at different angles of attack. Top: $\alpha = 14°$, $Re = 5.2 \cdot 10^4$; middle: $\alpha = 17°$, $Re = 8.0 \cdot 10^4$; bottom: $\alpha = 20°$, $Re = 5.2 \cdot 10^4$.

hydrofoil is in deep stall. Excitation with momentum coefficients up to $c'_\mu = 1.11\%$ results in an increase of C_L at $St_e = O(1)$. The C_L versus St_e curves exhibit the typical shape found for shear layer excitation. Forcing with $St_e \gtrsim 6$ has practically no effect on the lift. Corresponding to the lift increase, the drag rises at low excitation frequencies ($St_e \lesssim 3$) compared to the unforced case. Such a drag increase has been observed experimentally by Hsiao (2003), Melton et al. (2003), Melton et al. (2004), and in numerical investigations of Wu et al. (1998). As well, numerical results on separation control by time periodic Lorentz forces by Mutschke et al. (2004) show this effect. According to Hsiao (2003) the reason for the drag rise is an increase of the separation bubble size due to the forcing which results in a larger lift, but due to a broadened wake in an increased drag as well. Melton et al. (2004) attribute the drag increase to a "lock–in" of excitation frequency and the vortex shedding process. The momentum coefficients given in Fig. 8 indicate that the drag reaches a maximum value for a specific c'_μ. For larger momentum coefficients, the drag decreases.

All results presented so far have been achieved with a sinusoidal forcing, i.e., the alternating current used to feed the electrodes had a sinusoidal wave form. One of the main advantages of using Lorentz forces as momentum source consists in an easy access to modify the wave form of the excitation. For this purpose only the feed current has to be modulated accordingly. The differences in applying an excitation with a sinusoidal, triangular or rectangular wave form, which are readily available from standard frequency generators, have been examined.

Fig. 9 shows C_L and C_D versus the effective momentum coefficient c'_μ defined by Eq. (9) for $Re = 5.2 \cdot 10^4$, $\alpha = 20°$ and $St_e = 1.5$. As well known, the square root term in Eq. (10) evaluates to $\hat{j}/\sqrt{3}$ for triangular, $\hat{j}/\sqrt{2}$ for sinusoidal and $\hat{j}$ for rectangular wave forms, where $\hat{j}$ is the peak current density. Under the conditions utilized in Fig. 9, the difference in the wave form apparently does not influence the forcing effect, all measured points arrange to one curve.

The ΔC_L versus c'_μ plot in Fig. 9 shows a kink. This suggests to fit straight lines to the regions with obviously different slopes.

$$\begin{aligned} \Delta C_L &= 75.5 \cdot c'_\mu \text{ for } c'_\mu < 0.4 \cdot 10^{-2} \\ \Delta C_L &= 0.218 + 21.5 \cdot c'_\mu \text{ for } c'_\mu \geq 0.4 \cdot 10^{-2} \end{aligned} \quad (19)$$

These lines have been included into the figure. Their intersection at $c'_\mu = 0.4\%$ coincides quite well with the drag maximum $\Delta C_D \approx 0.07$. The initial steeper lift increase is therefore coupled to a drag rise, whereas the following weaker enlargement is accompanied by a decreasing drag.

Following the reasoning of Hsiao (2003) and the explanation and streamlines given by Wu et al. (1998) (esp. figs. 23-25 of this reference), size and position of the lifting vortex in the time averaged flow field is influenced by the excitation and can be used to explain the different behaviour. The integral force values given here suggest that at low excitation levels the lifting vortex is moved towards the foil, thereby increasing lift and drag. For larger excitation levels, the size of the mean separated region is more and more reduced, resulting in a drag decrease and further lift increase. However, without a detailed knowledge of the flow field, the scenario sketched above remains obviously speculative.

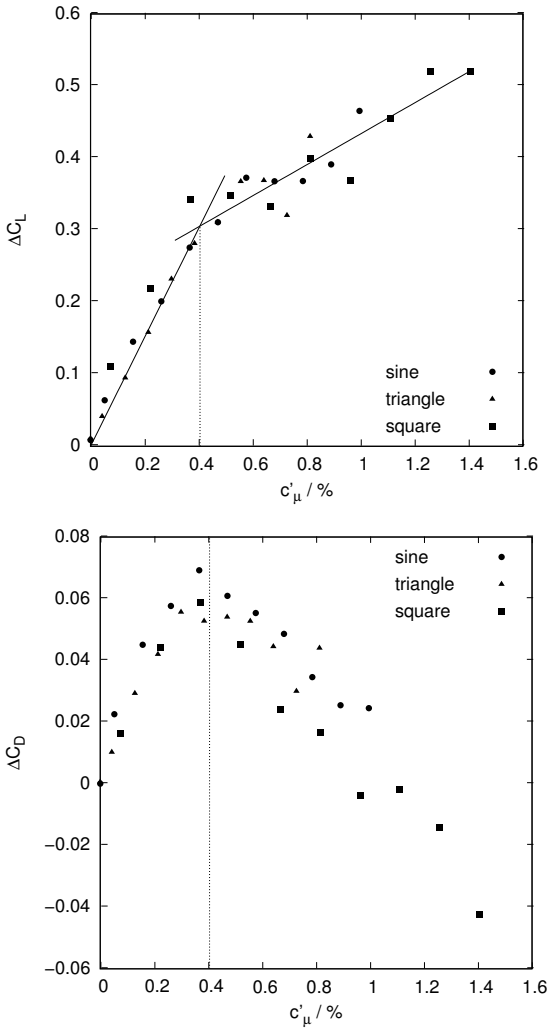

Figure 9: Lift (top) and drag (bottom) variation versus momentum coefficient for periodic electromagnetic excitation with different wave forms ($\alpha = 20°, St_e = 1.5, Re = 5.2 \cdot 10^4$). Including fitted lines (19).

Fig. 10 displays drag and lift coefficient versus excitation frequency for $Re = 1.06 \cdot 10^5$, $\alpha = 20°$ and a fixed $c'_\mu = 0.2\%$. Generally, the curve shape is similar to that

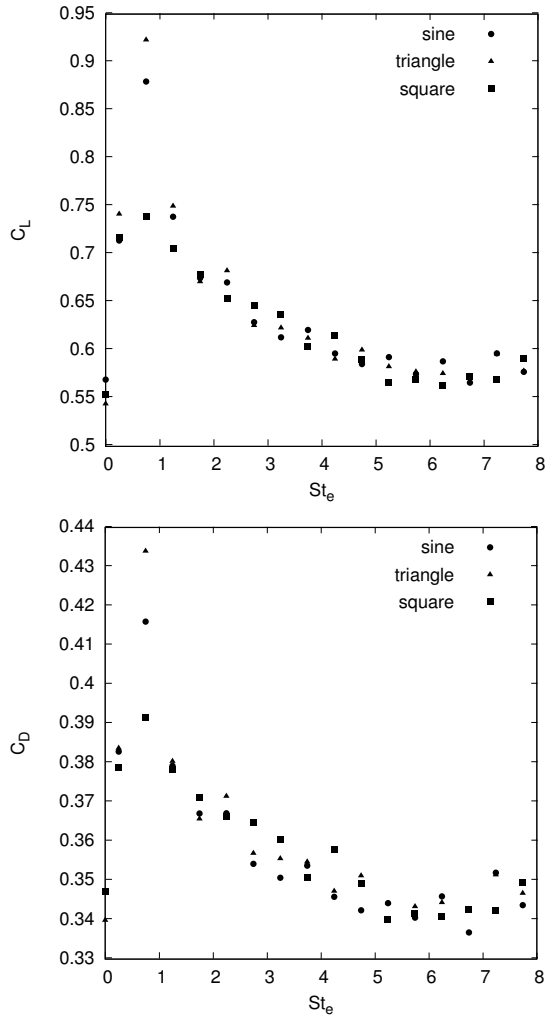

Figure 10: C_L and C_D versus excitation frequency for different wave forms $Re = 1.06 \cdot 10^5$, $\alpha = 20°$, $c'_\mu = 0.2\%$.

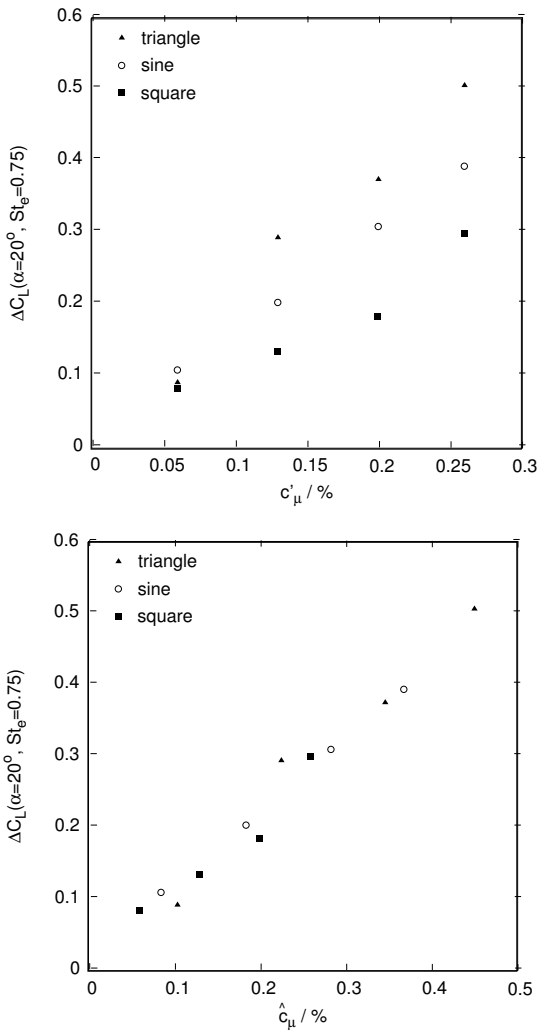

Figure 11: C_L increase at $Re = 1.06 \cdot 10^5$, $St_e = 0.75$ and $\alpha = 20°$ *versus* the efficient (top) and the peak (bottom) momentum coefficient.

shown in Fig. 8 for $Re = 5.2 \cdot 10^5$ and $\alpha = 20°$. For $St_e \geq 2$, no systematic influence of the excitation wave form on lift and drag appears. Unlike that, around the most efficient frequency of $St_e = 0.75$, the wave form has a very pronounced effect. Maximum values of lift and drag are obtained applying triangular waves, the maximum values are smaller for sinusoidal forcing and rectangular waves have the least effect.

The lift increment for excitation with the most effective frequency ($St_e = 0.75$) at $\alpha = 20°$and $Re = 1.06 \cdot 10^5$ is shown in Fig. 11 versus the effective momentum coefficient c'_μ (top) and the peak momentum coefficient $\hat{c}_\mu$ (bottom). $\hat{c}_\mu$ is the momentum coefficient defined with the peak value of the current density, i.e.

$$\hat{c}_\mu = \frac{1}{2} \cdot \frac{aB_0\hat{j}}{\rho U_\infty^2} \cdot \frac{x_e - x_s}{c}. \tag{20}$$

While the data follow distinct lines when ΔC_L is plotted versus the effective momentum coefficient, all data collapse fairly well in the ΔC_L versus $\hat{c}_\mu$ plot. That means, around the most effective excitation frequency not the effective, but the peak momentum input determines the attainable lift increase. If the validity of this statement will cease also for Dirac pulses, it certainly offers attractive prospects for an efficiency increase of periodic excitation arrangements. As can be inferred from Fig. 11 the lift increment for $c'_\mu = 0.26\%$ and excitation with a triangular wave form is approximately 70% larger than that reachable using a rectangular wave form.

Electromagnetic excitation has been shown to reproduce the characteristic frequency dependence of separation control by periodic blowing and suction. A comparison of the lift polar for electromagnetic forcing and that

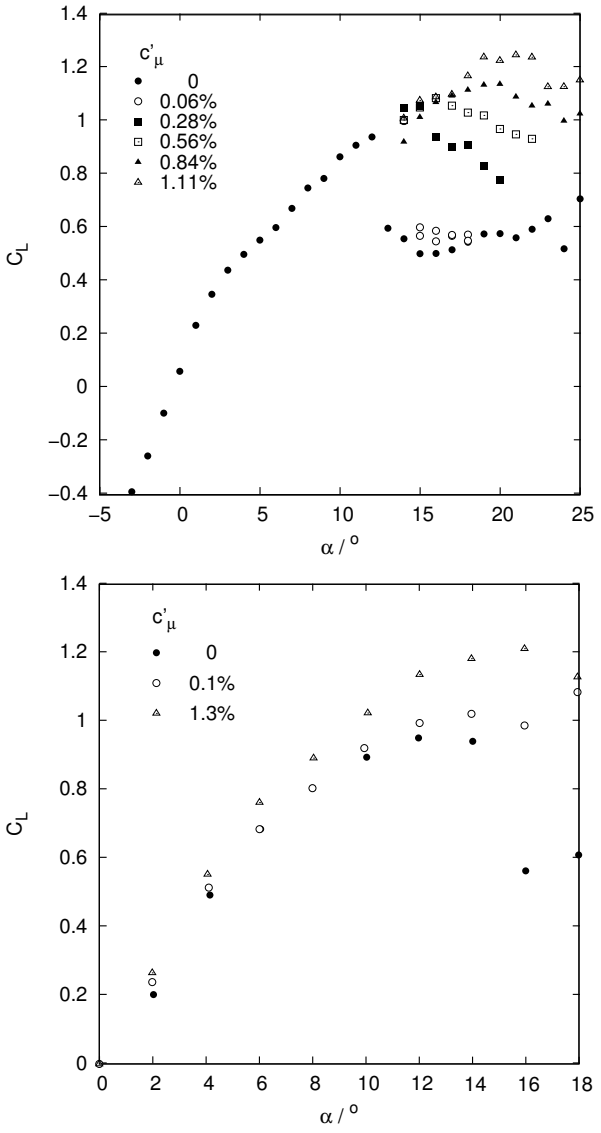

Figure 12: Electromagnetic excitation at $Re = 5.2 \cdot 10^4$, $St_e = 0.5$ (top) compared to oscillatory blowing from the leading edge of a NACA 0015 at $Re = 1.5 \cdot 10^5$, $St_e = 1.1$ (bottom). With permission from Greenblatt and Wygnanski (2000).

measured for oscillatory blowing from the leading edge of a NACA 0015 (figure 22a of Greenblatt and Wygnanski, 2000) gives Fig. 12. While Reynolds numbers and excitation frequencies differ, $Re = 5.2 \cdot 10^4$ and $St_e = 0.5$ for electromagnetic excitation and $Re = 1.5 \cdot 10^5$ and $St_e = 1.1$ for oscillatory blowing, respectively, the attained lift gain is comparable for similar momentum coefficients. The differences in the curves may be caused mainly by the different Re, aspect ratio and blockage. For electromagnetic forcing, already for the small momentum coefficient of $c'_\mu = 0.06\%$, stall is delayed from 13°to 15° due to a

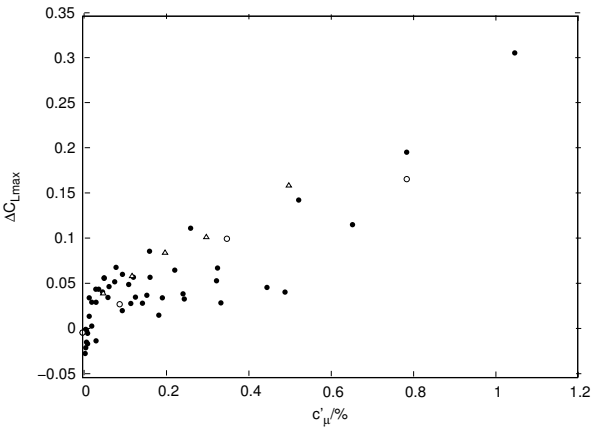

Figure 13: Maximum lift gain by electromagnetic excitation at $Re = 5.2 \cdot 10^4 \ldots 1.48 \cdot 10^5$, $St_e = 0.5$ (filled symbols) compared to oscillatory blowing from the leading edge of a NACA 0012 at $Re = 2.4 \cdot 10^5$, $St_e = 1.5$ (open symbols) and a Sikorsky SSC–A09 at $Re = 5 \cdot 10^5$, $St_e = 1.3$ (open triangles). With permission from Greenblatt and Wygnanski (2000) and McCormick (2000).

boundary layer transition triggered by the excitation. Lift values in the stalled region are only marginally increased as compared to the unforced flow. The picture changes for larger momentum coefficients, the abrupt stall merges into a more gentle one. C_L is considerably increased in the post stall region, but the maximum lift increases mainly due to higher critical angles of attack. In the pre–stall region, no data have been acquired for the forced flow, but judging from Fig. 8, only a very modest increase would be expected. Somewhat in contrast to this, for oscillatory blowing a lift increase may be found for almost all angles of attack. This effect might be related to the leading–edge discontinuity present at this airfoil, which has a slightly different geometry in the nose region than a real NACA 0015. The lift polar for a NACA 0012 at $Re = 2.4 \cdot 10^5$ and $St_e = 1.5$ given in figure 22b of Greenblatt and Wygnanski (2000) shows no distinct lift increase for angles of attack $\alpha < 8°$.

COMPARISION OF STEADY AND PERIODIC FORCES

For shipbuilding applications like rudders and stabilizer fins the lift gain relative to the separated flow is less important, the increase of the maximum attainable lift (17) in the full range of inclination angles is of primary interest. Fig. 13 shows this quantity versus the momentum coefficient in the Reynolds number range $5.2 \cdot 10^4 \leq Re \leq 1.48 \cdot 10^5$. For comparison, corresponding data for oscillatoty blowing from figure 23b of Greenblatt and Wygnanski (2000) obtained on a NACA 0012 foil for $Re =$

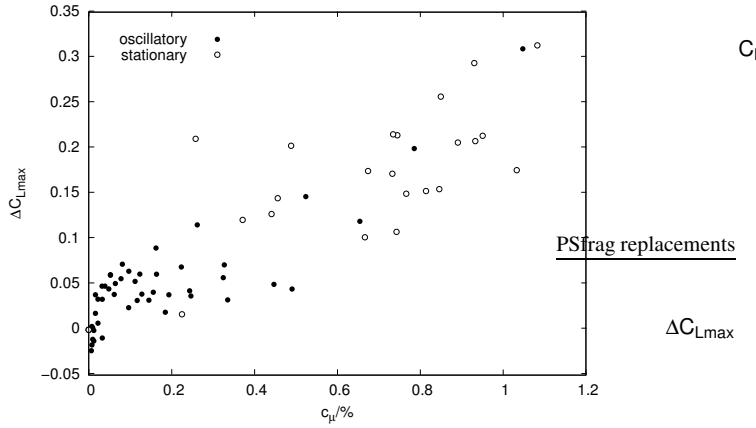

Figure 14: Maximum lift gain by electromagnetic forces: oscillatory excitation and stationary action compared.

$2.4 \cdot 10^5$ and $St_e = 1.5$ and from figure 14 of McCormick (2000) on a Sikorsky SSC–A09 foil for $Re = 5 \cdot 10^5$ and $St_e = 1.3$ have been included. The relatively large scatter of the data obtained for electromagnetic excitation is mainly a Reynolds number effect since in this range of *Re* laminar separation bubbles are expected to have a pronounced effect on the overall behavior of the flow. Despite these uncertainties, the data for oscillatory blowing show the same trend and fit in quite well regardless the differences in foil shape and Reynolds number.

The application of periodic momentum to control separated flows is usually expected to result in a comparable gain for a considerably lower expenditure than in case of steady momentum input (see e.g. Greenblatt and Wygnanski, 2000). In the case of electromagnetic forcing, this expectation is fulfilled if the lift gain for a fixed angle of attack is considered. Although no direct comparison in the frame of the data presented here is possible since steady Lorentz forces have not been applied to the NACA 0015_S, data from experiments with the PTL IV_S hydrofoil are available. They indicate a decrease of the momentum input necessary to recover the lift of a stalled hydrofoil by a factor of $7 \ldots 17$ compared to steady forcing. Fig. 14 shows the maximum attainable lift gain according to Eq. (17) for both steady as well as time periodic Lorentz forces versus the momentum coefficient. Data for steady forcing are taken from Weier et al. (2003) and belong to experiments with the PTL IV_S, PTL IV_L, and NACA 0015_L hydrofoils. Again the considerable scatter might be attributed to the Reynolds number range, different foil shapes, blockage and aspect ratios. However, there is certainly no efficiency gain of an order of magnitude for oscillatory excitation. As sketched in Fig. 15, in the case of steady forcing, lift is increased by two mechanisms: 1) reattaching the separated flow and therefore increasing the critical angle, and 2) introducing circulation due to acceleration of the attached suction side flow. Unlike that, no additional circulation in an already attached flow is generated in the case of periodic excitation. The fit of the ΔC_{Lmax} versus c_μ data for steady Lorentz forces (18) indicates that the added circulation ΔC_{Lcirc} contributes substantially to ΔC_{Lmax} in the case of the single element hydrofoils considered here. The case might be different for the high lift configurations with blowing over the flaps, and flap shoulder excitation, respectively. Additionally, unlike steady blowing a steady Lorentz force has no detrimental effect for low momentum coefficients.

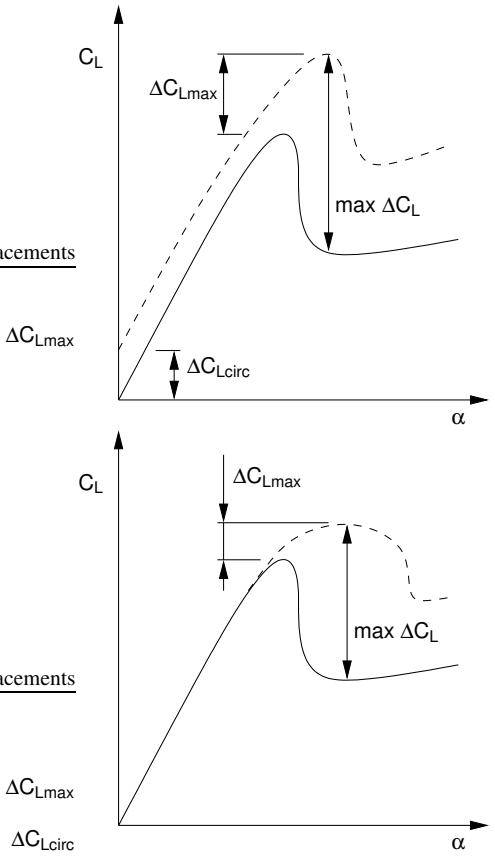

Figure 15: Schematic influence of a stationary (top) and a time periodic (bottom) Lorentz force on the maximum lift gain of a hydrofoil.

ENERGETICAL EFFICIENCY

As has been pointed out by e.g. Shatrov and Yakovlev (1992) the energetical efficiency η of momentum generation by electromagnetic forces is inversly proportional to the load factor (4). This can be shown easily for the cases considered here, if we follow Greenblatt and Wygnanski (2000) and define an input power coefficient as

$$C_E = \frac{W_i}{\frac{\rho}{2} csU_\infty^3}, \tag{21}$$

with the electrical input power W_i. The electrical input power can be calculated from the ohmic resistance of the electrode assembly R (7) and the total current I to

$$W_i = \overbrace{\frac{4a}{s(x_e-x_s)\sigma}}^{R} \overbrace{j_0^2\frac{s^2(x_e-x_s)^2}{16}}^{I^2}. \quad (22)$$

For the efficiency of electromagnetic momentum generation η it follows with $j_0 = \sigma E_0$:

$$\eta = \frac{c'_\mu}{C_E} = \frac{B_0 U_\infty \sigma}{j_0} = \frac{1}{\phi}. \quad (23)$$

This situation is not different from that found in MHD ship propulsion (Convert and Thibault, 1994). Due to the use of rare earth permanent magnets, the available magnetic induction B_0 is relatively small and we have to apply large electric fields and therefore large load factors ϕ. A consequence is the low efficiency of momentum generation. An order of magnitude estimate with $\sigma = O(1)$ S/m, $U_\infty = O(1)$ m/s, $B_0 = O(10^{-1})$ T and $j_0 = O(10^4)$ A/m^2 results in $\eta = O(10^{-5})$ and corresponds well to the experimental values of Breuer et al. (2004). Since the efficiency of momentum generation is very low, the overall efficiency of the control is very low as well. This is readily seen from the definition of the *hydrofoil efficiency including the electric power input* (see Greenblatt and Wygnanski, 2000)

$$\eta_{\text{foil+input}} = \frac{C_L}{C_D + C_E} \quad (24)$$

with C_L and C_D denoting the lift and drag coefficient, respectively. While the *hydrofoil only efficiency* (see Greenblatt and Wygnanski, 2000)

$$\eta_{\text{foil only}} = \frac{C_L}{C_D + c'_\mu} \quad (25)$$

should be comparable to that found by conventional excitation methods, the efficiency of momentum generations leads to a very low $\eta_{\text{foil+input}}$.

This said, there is hardly an *energetical* advantage over conventional means when using Lorentz forces for periodic excitation in low conducting media and with moderate magnetic field strength. However, the actuator itself possess several distinct features, mentioned in the introduction, not easily reproducable by other means. These features, especially the unlimited frequency response and the possibility to realise a multitude of wave forms makes the Lorentz force actuator an attractive research tool. The lessons learned from different kinds of momentum input found with the electromagnetic actuation, can later be used to design conventional actuators with much better energetical efficiency.

On the other hand, the actuator efficiency for a fixed momentum input ($\sim j_0 B_0$) increases quadratically with the applied magnetic field strength as can be seen from (23). Therefore, with strong enough magnetic fields, an actuator with a power consumption acceptable even for practical purposes would be possible. However, if the load factor decreases, condition (5) will be violated and the Lorentz force then depends upon the flow. It has already been shown numerically by Shatrov and Gerbeth (2004) that the energetical efficiency of turbulent skin friction reduction by a Lorentz force oscillating in spanwise direction can be considerably improved for load factors $\phi \sim 1$ compared to $\phi \sim 1000$.

CONCLUSIONS

The influence of stationary and time periodic wall–parallel Lorentz forces on the flow around hydrofoils has been studied in electrolyte flows (saltwater and dilute NaOH) in the Reynolds number range $3 \cdot 10^4 < Re < 3.7 \cdot 10^5$.

With stationary Lorentz forces, separation as well as circulation can be readily controlled. If the Lorentz force acts on an already attached flow, the lift increase is proportional to the square root of the momentum coefficient, while the drag decreases linearly with increasing momentum coefficient. The lift increase is more pronounced, if the Lorentz force leads to a reattachement of an otherwise separated suction side flow.

Time periodic Lorentz forces show essential features like characteristic excitation frequencies, effective momentum coefficients and resulting lift gains comparing well to that found with other methods of periodic excitation.

A specific lift increase with respect to the value of the separated flow can be obtained by oscillatory forcing with fractions of the momentum input necessary for steady Lorentz forces. In contrast, an equal increase of the maximum lift gain requires a similar expenditure for both control methods.

The Lorentz force gives a great flexibility in chosing the time dependency of the forcing. The aplication of wave forms different from sinusoidal ones has been found to increase the efficiency under certain conditions by up to 70% compared to a sinusoidal forcing. That offers a potential for further energetic optimization of the flow control by unsteady Lorentz forces.

An energetically favourable use of Lorentz forces in fluids of low electrically conductivity is unlikely for the hitherto almost exclusively investigated range of high load factors. The application of strong magnetic fields seems unavoidable, if qualitative improvements are to be achieved.

ACKNOWLEDGEMENTS

We thank David Greenblatt and Duane C. McCormick for the friendly permission to use their data and Fei–Bin Hsiao for fruitful discussion. Financial support from Deutsche Forschungsgemeinschaft (DFG) in frame of the Collaborative Research Centre (SFB) 609 is gratefully acknowledged.

REFERENCES

Avilov, V., "Electric and magnetic fields for the Riga Plate," 1998, FZR Internal Report.

Berger, T.W., Kim, J., Lee, C., and Lim, J., "Turbulent boundary layer control utilizing the Lorentz force," Phys. Fluids, vol. 12, no. 3, 2000, pp. 631–649.

Breuer, K., Park, J., and Henoch, C., "Actuation and control of a turbulent channel flow using Lorentz forces," Phys. Fluids, vol. 16, no. 4, 2004, pp. 897–907.

Chen, Z. and Aubry, N., "Active control of cylinder wake," Communications in Nonlinear Science and Numerical Simulation, vol. 10, 2005, pp. 205–216.

Convert, D. and Thibault, J., "External MHD Propulsion," 2^{nd} Int. Conf. Energy Transfer in MHD Flows. Aussois, France, 1994, pp. 521–530.

Crausse, É. and Cachon, P., "Actions électromagnétiques sur les liquides en mouvement, notamment dans la couche limite d' obstacles immergés," Comptes rendus hebdomadaires des séances de l' Académie des Sciences, vol. 238, 1954, pp. 2488–2490.

Crawford, C.H. and Karniadakis, G.E., "Reynolds stress analysis of EMHD–controlled wall turbulence. Part I. Streamwise forcing," Phys. Fluids, vol. 9, 1997, pp. 788–806.

Du, Y., Symeonidis, V., and Karniadakis, G., "Drag reduction in wall–bounded turbulence via a transverse travelling wave," J. Fluid Mech., vol. 457, 2002, pp. 1–34.

Gad–el–Hak, M. and Bushnell, D.M., "Separation Control: Review," J. Fluids Engng., vol. 113, 1991, pp. 5–30.

Gailitis, A. and Lielausis, O., "On a possibility to reduce the hydrodynamic resistance of a plate in an electrolyte," Appl. Magnetohydrodynamics, Rep. Phys. Inst., vol. 12, 1961, pp. 143–146, (in Russian).

Greenblatt, D. and Wygnanski, I., "The control of flow separation by periodic excitation," Prog. Aero. Sci., vol. 36, 2000, pp. 487–545.

Grienberg, E., "On determination of properties of some potential fields," Applied Magnetohydrodynamics. Reports of the Physics Institute, vol. 12, 1961, pp. 147–154, (in Russian).

Henoch, C. and Stace, J., "Experimental investigation of a salt water turbulent boundary layer modified by an applied streamwise magnetohydrodynamic body force," Phys. Fluids, vol. 7, 1995, pp. 1371–1383.

Hsiao, F.B., private communication, 2003.

Hsiao, F.B., Liu, C.F., and Shyu, J.Y., "Control of Wall–Separated Flow by Internal Acoustic Excitation," AIAA Journal, vol. 28, no. 8, 1990, pp. 1440–1446.

Kim, S. and Lee, C., "Investigation of the flow around a circular cylinder under the influence of an electromagnetic force," Exp. Fluids, vol. 28, 2000, pp. 252–260.

Lielausis, O., Effect of electromagnetic forces on the flow of liquid metals and electrolytes, Ph.D. thesis, Academy of Sciences of the Latvian SSR, Institute of Physics, Riga, 1961, (in Russian).

McCormick, D.C., "Boundary Layer Separation Control with Directed Synthetic Jets," 38^{th} AIAA Aerospace Sciences Meeting & Exhibit, Reno, NV, 2000, also as AIAA–2000–0519 paper.

Melton, L., Yao, C.S., and Seifert, A., "Active Control of Separation From the Flap of a Supercritical Airfoil," 33^{rd} AIAA Fluid Dynamics Conference, Orlando, FL, 2003, also as AIAA–2003–4005 paper.

Melton, L., Yao, C.S., and Seifert, A., "Application of Excitation from Multiple Locations on a Simplified High–Lift System," 2^{nd} Flow Control Conference, Portland, OR, 2004, also as AIAA–2004–2324 paper.

Meyer, R., "Magnetohydrodynamic method and apparatus," US Patent 3,360,220, 1967.

Motora, S. and Takezawa, S., "Development of MHS ship propulsion and results of sea trials of an experimental ship YAMATO–1," 2^{nd} Int. Conf. Energy Transfer in MHD Flows, Aussois, France, 1994, pp. 501–510.

Mutschke, G., Gerbeth, G., Albrecht, T., and Grundmann, R., "Separation Control at hydrofoils using Lorentz forces," Eur. J. Mech. B Fluids, submitted.

Nosenchuck, D. and Brown, G., "Discrete spatial control of wall shear stress in a turbulent boundary layer," In So, R., Speziale, C., and Launder, B., eds., Near–Wall Turbulent Flows, Elsevier, 1993, pp. 689–698.

Nosenchuck, D., Brown, G., Culver, H., Eng, T., and Huang, I., "Spatial and Temporal Characteristics of Boundary Layers Controlled with the Lorentz Force," 12^{th} Australian Fluid Mechanics Conference, Sydney, 1995.

O'Sullivan, P. and Biringen, S., "Direct numerical simulations of low Reynolds number turbulent channel flow with EMHD control," Phys. Fluids, vol. 10, no. 5, 1998, pp. 1169–1181.

Pang, J. and Choi, K.S., "Turbulent drag reduction by Lorentz force oscillation," Phys. Fluids, vol. 16, no. 5, 2004, pp. L35–L38.

Petit, J.P., "Is supersonic flight, without shock wave, possible?" Proceedings of the 8th International Conference on MHD Electrical Power Generation, Moscow, 1983, pp. 74–77.

Poisson-Quinton, P., "Einige physikalische Betrachtungen über das Ausblasen an Tragflügeln," Jahrbuch der WGL, 1956, pp. 29–51.

Posdziech, O. and Grundmann, R., "Electromagnetic control of seawater flow around circular cylinders," European Journal of Mechanics–B/Fluids, vol. 20, 2001, pp. 255–274.

Resler, E.L., Jr and Sears, W.R., "The Prospects for Magneto–Aerodynamics," J. Aero. Sci., vol. 25, 1958, pp. 235–245,258.

Rice, W., "Propulsion system," US Patent 2,997,013, 1961.

Rossi, L. and Thibault, J.P., "Investigation of wall normal electromagnetic actuator for seawater flow control," J. Turbulence, vol. 3, 2002, no. 005.

Rossow, V.J., "On flow of electrically conducting fluids over a flat plate in the presence of a transverse magnetic field," Tech. Rep. TN 3971, NACA, 1957.

Schwier, W., "Blasversuche zur Auftriebssteigerung am Profil 23015 mit verschiedenen Klappenformen," Tech. Rep. FB 1865, Zentrale f. wiss. Berichtswesen, Berlin–Adlershof, 1943.

Shatrov, V. and Gerbeth, G., "Magnetohydrodynamic drag reduction and efficiency," Int. Workshop on Flow Control by Tailored Magnetic Fields, Dresden, 2004.

Shatrov, V. and Gerbeth, G., "Electromagnetic flow control leading to a strong drag reduction of a sphere," Fluid Dynamics Research, 2005, in press.

Shatrov, V. and Yakovlev, V., "Optimization of the internal source in the problem of MHD flow around a sphere," J. Applied Mechanics and Technical Physics, vol. 33, 1992, pp. 334–341.

Shercliff, J.A., A textbook of magnetohydrodynamics. Pergamon Press, Oxford, 1965.

Shtern, A., "Feasibility of modifying the boundary layer by crossed electric and magnetic fields," Magnitnaya Gidrodinamika, vol. 6, no. 3, 1970, pp. 124–128.

Siestrunck, R., "General theory of the jet flap in two–dimensional flow," In Lachmann, G., ed., Boundary Layer and Flow Control, vol. 2. Pergamon Press, 1961, pp. 342–364.

Sutton, G. and Sherman, A., Engineering Magnetohydrodynamics. McGraw Hill, New York, 1965.

Thibault, J.P. and Rossi, L., "Electromagnetic flow control: characteristic numbers and flow regimes of a wall–normal actuator," J. Phys. D: Appl. Phys., vol. 36, 2003, pp. 2559–2568.

Tsinober, A.B. and Shtern, A.G., "On the possibility to increase the stability of the flow in the boundary layer by means of crossed electric and magnetic fields," Magnitnaya Gidrodinamica, vol. 3, no. 2, 1967, pp. 152–154. (in Russian).

Weier, T., Fey, U., Gerbeth, G., Mutschke, G., Lielausis, O., and Platacis, E., "Boundary layer control by means of wall parallel Lorentz forces," Magnetohydrodynamics, vol. 37, no. 1/2, 2001, pp. 177–186.

Weier, T. and Gerbeth, G., "Control of separated flows by time periodic Lorentz forces," . Eur. J. Mech. B Fluids, vol. 23, 2004, pp. 835–849.

Weier, T., Gerbeth, G., Mutschke, G., Lielausis, O., and Lammers, G., "Control of Flow Separation Using Electromagnetic Forces," Flow, Turbulence and Combustion, vol. 71, 2003, pp. 5–17.

Weier, T., Gerbeth, G., Mutschke, G., Platacis, E., and Lielausis, O., "Experiments on cylinder wake stabilization in an electrolyte solution by means of electromagnetic forces localized on the cylinder surface," Experimental Thermal and Fluid Science, vol. 16, 1998, pp. 84–91.

Wu, J.Z., Lu, X.Y., Denny, A., Fan, M., and Wu, J.M., "Post–stall flow control on an airfoil by local unsteady forcing," J. Fluid Mech., vol. 371, 1998, pp. 21–58.

Wygnanski, I. and Seifert, A., "The control of separation by periodic oscillations," AIAA-Paper 94–2608, 1994.